Available online at www.sciencedirect.com

ScienceDirect

journal homepage: www.elsevier.com/locate/he

Fabrication of graphene/$CaIn_2O_4$ composites with enhanced photocatalytic activity from water under visible light irradiation

Jianjun Ding [a,b], *Wenhao Yan* [a,b], *Song Sun* [a,b], *Jun Bao* [a,b], *Chen Gao* [a,b,*]

[a] *National Synchrotron Radiation Laboratory and Collaborative Innovation Center of Chemistry for Energy Materials, University of Science and Technology of China, Hefei, Anhui 230029, China*

[b] *CAS Key Laboratory of Materials for Energy Conversion, Department of Materials Science and Engineering, University of Science and Technology of China, Hefei, Anhui 230026, China*

ARTICLE INFO

Article history:
Received 16 August 2013
Received in revised form
6 October 2013
Accepted 15 October 2013
Available online 8 November 2013

Keywords:
Graphene
$CaIn_2O_4$
Composite
Solvothermal
Visible light photocatalysis

ABSTRACT

A series of graphene/$CaIn_2O_4$ composites were synthesized using a facile solvothermal method to improve the photocatalytic performance of $CaIn_2O_4$. The reduction of graphene oxide to graphene and the deposition of $CaIn_2O_4$ nanoparticles on the graphene sheets can be achieved simultaneously during the solvothermal process. The photocatalytic activities of as-prepared graphene/$CaIn_2O_4$ composites for hydrogen evolution from CH_3OH/H_2O solution were investigated under visible light irradiation. It was found that graphene exhibited an obvious influence on the photocatalytic activity of $CaIn_2O_4$. The graphene/$CaIn_2O_4$ composite reached a high H_2 evolution rate of 62.5 μmol h^{-1} from CH_3OH/H_2O solution when the content of graphene was 1 wt%. Furthermore, the 1 wt% graphene/$CaIn_2O_4$ composite did not show deactivation for H_2 evolution for longer than 32 h. This work could provide a new insight into the fabrication of visible light driven photocatalysts with efficient and stable performance.

1. Introduction

Hydrogen fuel has been recognized as an environmental friendly renewable source for the future. Since photoelectron-chemical splitting of water was reported by Fujishima and Honda in 1972 [1], the production of hydrogen using photocatalyst has received a lot of attention. Among the semiconductor photocatalysts, TiO_2 is the most widely used photocatalyst due to its non-toxicity, good stability and excellent photocatalytic activity [2,3]. However, the relatively wide band gap of TiO_2 (3.2 eV for anatase) limits the utilization, which accounts for only 4% of the incoming solar energy. Therefore, development of visible-light-driven photocatalysts becomes critical in current photocatalysis research, because visible light contributes to about 43% of the solar spectrum.

Metal oxides are potential candidates for visible-light-driven photocatalysts, and promising results have been reported for WO_3 [4], $BiVO_4$ [5], $In_{1-x}Ni_xTaO_4$ [6], $CaBi_2O_4$ [7], etc. $CaIn_2O_4$ is a ternary semiconductor oxide that belongs to the AB_2O_4 family of ternary compounds. It is considered as a potential eco-friendly and visible-light-driven photocatalyst for

* *Corresponding author*. National Synchrotron Radiation Laboratory and Collaborative Innovation Center of Chemistry for Energy Materials, University of Science and Technology of China, Hefei, Anhui 230029, China. Tel.: +86 551 63602031; fax: +86 551 65141078.
E-mail address: cgao@ustc.edu.cn (C. Gao).

http://dx.doi.org/10.1016/j.ijhydene.2013.10.077

the degradation of organic pollutants although its light absorption ability is weak [8–15]. We previously reported that a type of $CaIn_2O_4$ nanorods was synthesized using a low temperature solution combustion method followed by a post-calcination process [16]. The nanorods shows better visible photocatalytic activity for methylene blue degradation, toluene oxidation and water decomposition than that of the sample synthesized by the conventional solid–state reaction. However, the efficiency for H_2 evolution from water splitting is still far from satisfactory. It is therefore highly desirable to develop a new modification that can enhance the photocatalytic activity of $CaIn_2O_4$.

Graphene is a two-dimensional π–conjugation sheet of carbon atoms bonded through sp^2 hybridization. Its remarkable electrical conductivity, large theoretical surface area, high chemical and thermal stability, and flexible structure have attracted great interest. During the past few years, numerous attempts have been made to combine graphene with semiconductor photocatalysts to enhance their photocatalytic performances [17–23]. Li Q et al. [24] pointed out that CdS/graphene composite was a highly efficient visible-light-driven photocatalyst for hydrogen production with apparent quantum efficiency of 22.5% at wavelength of 420 nm. Cheng P et al. [25] synthesized a TiO_2/graphene composite and applied it as the photocatalyst in hydrogen evolution under irradiation of UV–Vis light, obtaining a maximum H_2 evolution rate of 668 μmol/h. Tang XS et al. [26] demonstrated that CuInZnS/graphene composite shows an enhancement of photocatalytic activity for hydrogen evolution in comparison with pure CuInZnS. As an excellent supporting matrix for photocatalysts, graphene can efficiently facilitate the charge separation and transportation from photocatalysts to graphene, suppress the recombination of photogenerated electrons and holes, and therefore enhance the photocatalytic performance.

In this work, we present a general approach for the preparation of graphene/$CaIn_2O_4$ composites in ethanol using graphene oxide as a precursor for graphene under solvothermal reaction. During the solvothermal process, the reduction of graphene oxide to graphene and the deposition of $CaIn_2O_4$ nanoparticles on the graphene sheets can be achieved simultaneously. The introduction of graphene can reduce the probability of electron–hole recombination and improve the separation efficiency. As a result, highly enhanced performance for hydrogen production was achieved using the obtained graphene/$CaIn_2O_4$ composite as the photocatalyst. Under visible light irradiation, the maximum hydrogen evolution rate achieved was 62.5 μmol h^{-1} from CH_3OH/H_2O solution when the content of graphene is 1 wt%, which was 6.6 times higher than that of pure CIO. This study shows a facile way to fabricate graphene-based semiconductor photocatalysts with high efficiency.

2. Experimental sections

2.1. Chemicals and materials

Indium nitrate was purchased from Aladdin Industrial Inc. Natural graphite powder, Calcium nitrate and glycine were supplied by Sinopharm Chemical Reagent Co., Ltd. All other reagents were at least of analytic reagent grade and used without further purification.

2.2. Synthesis of $CaIn_2O_4$

$CaIn_2O_4$ (CIO) was synthesized by a low temperature solution combustion method, which was also used in our previous study [16]. Briefly, 0.71 g $Ca(NO_3)_2 \cdot 4H_2O$, 1.8 g $In(NO_3)_3$ and 1.0 g $C_2H_5NO_2$ were dissolved in 30 mL deionized water. The solution was left in air more than 24 h for diffusion. After that, the mixed solution was placed in an electrical furnace at 473 K for 30 min, and then slowly heated to 623 K in 50 min. During this period, a spontaneous combustion took place and a fluffy powder was formed. At last, the powder was annealed at 1373 K for 12 h in air.

2.3. Fabrication of graphene/$CaIn_2O_4$ composite photocatalysts

The graphene/$CaIn_2O_4$ (G/CIO) composites were obtained by a solvothermal method. In a typical process, a given amount of graphene oxide (GO, prepared from natural graphite powder by the modified Hummers' method [27]) was dissolved in 80 mL of absolute ethanol under ultrasonic shaking for several hours to obtain a well-dispersed GO suspension. Then, 500 mg of as-prepared CIO powder was added to the calculated amount of the above GO solution to prepare 0.5, 1, 2, and 5 wt% G/CIO with different weight ratios of graphene. The mixed solution was stirred for 1 h to obtain a homogenous suspension. Next, the suspension was transferred to a 100 mL Teflon-lined stainless steel autoclave with up to 80% of the total volume. The autoclave was sealed and kept at 453 K for 12 h to simultaneously achieve the reduction of GO and the deposition of CIO nanoparticles on the graphene substrate. Finally, the product was collected and washed using absolute ethanol and deionized water several times before drying at 353 K. In addition, the bare graphene sample without any CIO powder was prepared under the same experimental conditions for comparison. The samples with different contents of graphene to CIO (0, 0.5, 1, 2 and 5 wt%) were labeled as G0/CIO, G0.5/CIO, G1/CIO, G2/CIO and G5/CIO, respectively.

2.4. Characterization

The surface characterization was carried out using X-ray Photoelectron Spectroscopy (XPS, ESCALAB 250, Thermo-VG Scientific) with a base pressure lower than 1.0×10^{-10} Pa and MgKα radiation ($E = 1253.6$ eV) operated at 150 W as the X-ray source. Raman spectra were recorded with an InVia microscopic confocal Raman spectrometer using a 514.5 nm laser beam. Powder X-ray diffraction (XRD) patterns were measured using a Rigaku D/max-γA rotation anode diffractometer with CuKα radiation ($\lambda = 0.15148$ nm) at a scan rate of 5° min^{-1} to determine the crystal phase of the prepared samples. The average grain size was calculated using the Scherrer's equation of three prominent XRD lines with correction for instrumental line broadening. The BET surface area was determined by an adsorption-desorption method (Micromeritics ASAP 2000) with N_2 as the adsorbent.

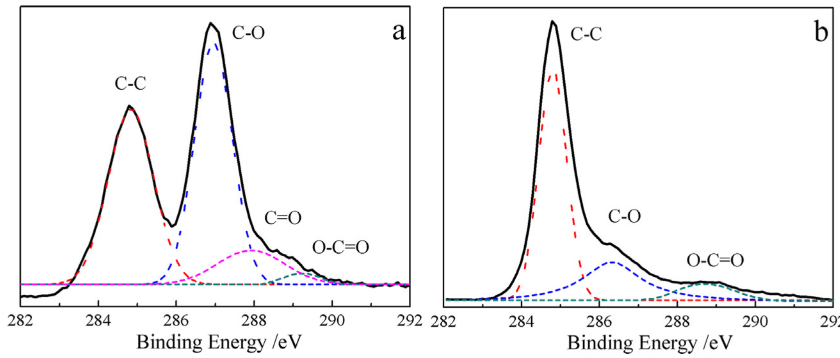

Fig. 1 – High-resolution XPS spectra of C1s from GO (a) and graphene (b).

Transmission electron microscopy (TEM) images were taken on a Hitachi H-800 TEM operating at 200 kV. The UV/Vis diffuse reflectance spectrum was measured at room temperature using a UV/Vis spectrometer (SolidSpec-3700, Shimadzu, Japan) using $BaSO_4$ as the reference.

2.5. *Photocatalytic experiments*

The photocatalytic activity for water splitting was measured in a 330 mL top-irradiation gas-closed circulation reactor. Photoirradiation was carried out using a 300 W Xe arc lamp (PLS-SXE 300, ChangTuo Ltd.) through Infrared and UV cutoff filters to ensure visible illumination only (420 nm $\leq \lambda \leq$ 750 nm). The distance between the lamp and the solution surface was 30 cm.

In a typical photocatalytic experiment, 20 mg of the photocatalyst was added into the reactor with constant stirring in a 120 mL CH_3OH/H_2O (CH_3OH: 20 mL, H_2O: 100 mL) solution. To eliminate any thermal effect, a water jacket outside the reactor was used to keep the temperature of the solution constant at room temperature by flowing cooling water. Before the reaction, the circulation system was purged with Argon several times to remove the dissolved oxygen. The H_2 evolved was analyzed using an online TCD gas chromatograph (Shimadzu GC 14C, Argon as a carrier gas, equipped with a TDX01 column). The amount of H_2 evolution was calculated versus the amount of photocatalyst in the system.

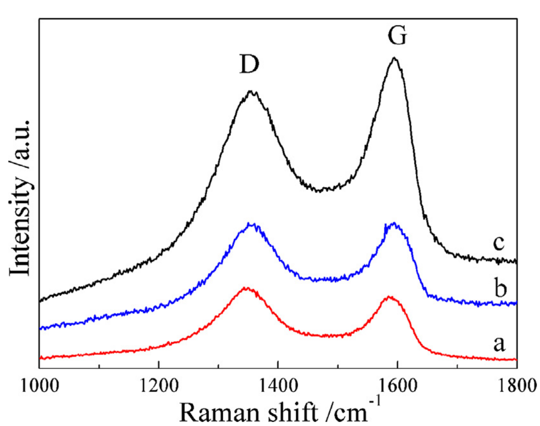

Fig. 2 – Raman spectra of GO (a), graphene (b) and G1/CIO composite (c).

3. Results and discussion

3.1. *Structures and morphology characterizations*

XPS was used to investigate the reduction degree of GO to graphene after the solvothermal process (Fig. 1). The XPS spectrum of C1s from GO (Fig. 1a, solid line) can be deconvoluted into four smaller peaks (dashed lines), which are

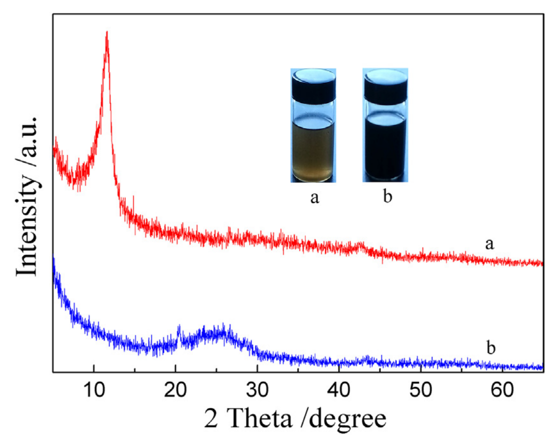

Fig. 3 – XRD patterns and photographs of GO (a) and graphene (b).

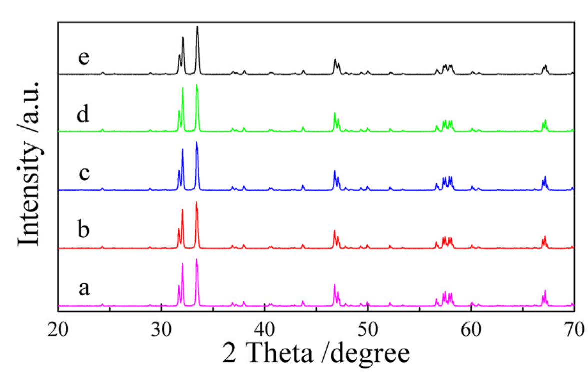

Fig. 4 – XRD patterns of G0/CIO (a), G0.5/CIO (b), G1/CIO (c), G2/CIO (d) and G5/CIO (e) composites.

Table 1 – Average grain sizes and BET surface areas of the synthesized G/CIO composites.

Sample	Graphene content (wt%)	Average grain size (nm)	BET surface area ($m^2\ g^{-1}$)
G0/CIO	0	48	2.74
G0.5/CIO	0.5	46	3.01
G1/CIO	1	45	3.61
G2/CIO	2	46	4.43
G5/CIO	5	42	6.98

ascribed to the following functional groups: C–C (sp^2 bonded carbon, 284.8 eV), C–O (epoxy/hydroxyl, 286.9 eV), C=O (carbonyl, 287.9 eV), and O–C=O (carboxyl, 289.4 eV), indicating a considerable degree of graphene oxidation [28–30]. After the solvothermal process, the significant decrease of oxygen-containing functional groups is observed based on the C1s XPS spectrum of graphene sample (Fig. 1b, solid line), and the C=O peak almost vanished, indicating the partial removal of the oxygen-containing functional groups [24]. Furthermore, the degree of GO can be quantified by calculating the relative content of carbon in the samples [31]. Briefly, GO has 40.4% graphitic carbon and 59.6% oxidized carbon, while it is 62.5% graphitic carbon and 37.5% oxidized carbon for graphene. These results indicate the sufficient reduction of GO to graphene by the solvothermal reduction treatment.

The structural changes from GO to graphene after the solvothermal process are also reflected in their Raman spectra (Fig. 2). As can be seen in Fig. 2, two characteristic peaks in the spectrum of GO are named as the D band at 1350 cm^{-1} and the G band at 1580 cm^{-1}. The D band is ascribed to local defects or disorders, while the G band arises from the sp^2 hybridized graphene domains. The D and G band of graphene were roughly at the similar position to those of GO. However, the I_D/I_G ratio of graphene decreased to 0.9 from 1.1 for GO, which proves more graphitization of graphene after the solvothermal process [32,33]. It is worth noting that a G band redshift from 1587 to 1595 cm^{-1} was observed for G1/CIO composite compared with GO. The phenomenon was similar to previous studies that the p-type doping of the graphene caused red-shift of the G band, indicating the charge transfer between graphene and CIO [34,35].

The X-ray diffraction patterns of GO, graphene and G/CIO composites are shown in Fig. 3 and Fig. 4. The GO sample exhibited an intensive peak at 11.6° (Fig. 3a), corresponding to an interlayer spacing of 0.76 nm calculated by the Bragg formula, which indicates the presence of oxygen-containing functional groups [36]. As for graphene sample (Fig. 3b), the diffraction peak at 11.6° disappeared and a very broad diffraction peak at ~25° appeared, demonstrating that almost all GO sheets have been reduced to graphene with a random packing and less functionalities [37]. In addition, from the photograph shown in the inset of Fig. 3, the color of GO and graphene dispersed in ethanol is remarkably different. The GO dispersion exhibits a brilliant yellow color, while the color of graphene dispersion is black, which indicates the richness of oxygen-containing functional groups on the surface of GO [29]. From Fig. 4, the main diffraction peaks of CIO are at 31.7°, 32.0°, 33.4°, 46.8° and 47.1° corresponding to the diffractions of the (040), (320), (121), (241) and (401) planes of orthorhombic-

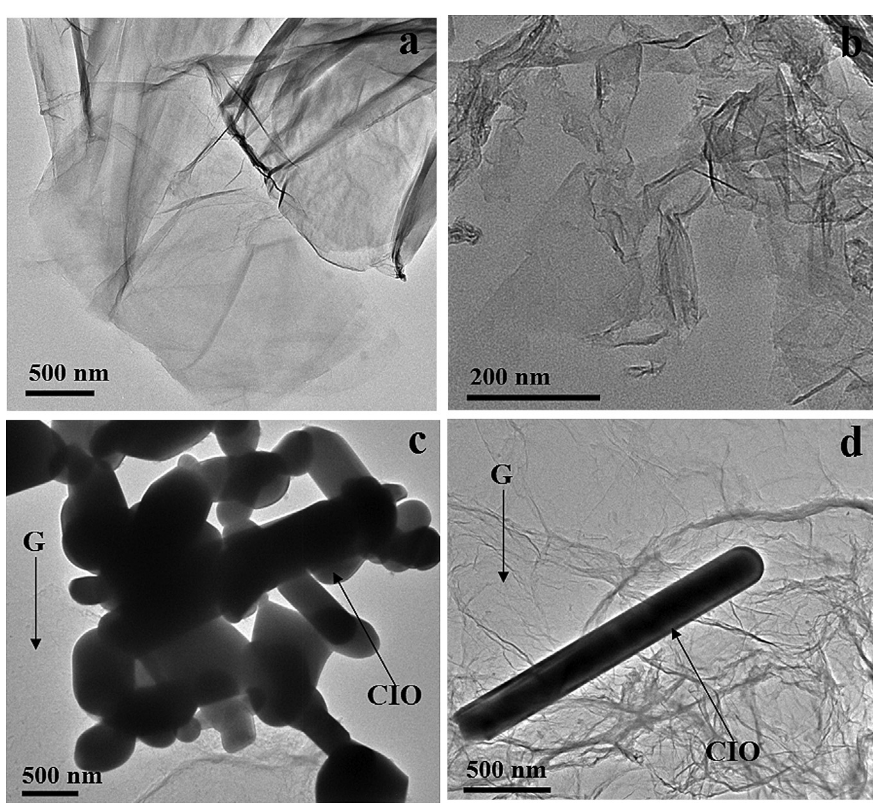

Fig. 5 – The TEM images of GO (a), graphene (b) and G1/CIO composite (c–d).

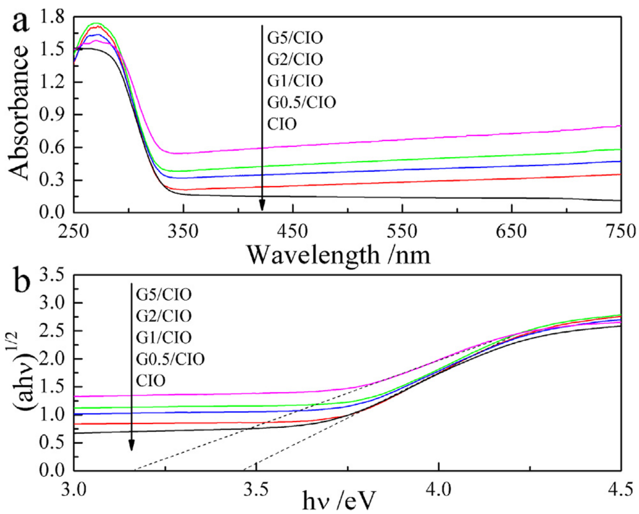

Fig. 6 – UV–Vis diffuse reflectance spectra of G/CIO composites (a), and plot of $(\alpha h\nu)^{1/2}$ versus photo energy (b).

type CIO (PCPDF #17-0643) respectively. All the diffraction peaks of G/CIO composites with different graphene content are similar to that of pure CIO. No characteristic diffraction peaks for carbon species are observed in the XRD patterns because of the low amount and relatively low diffraction intensity of graphene [38]. The average grain sizes and specific surface areas of the G/CIO composites with different content of graphene are listed in Table 1. It can be seen that the BET surface area increased gradually from 2.74 to 4.98 $m^2\ g^{-1}$ with increasing graphene content, while the average grain size of the composites was similar to that of the pure CIO. The larger surface area of the composites could be beneficial for enhancing the photocatalytic activity of the composites studied.

TEM image of GO (Fig. 5a) reveals flexible and crumpled sheets resulting from the deformation and distortion of graphite sheets during the oxidation reaction. After the solvothermal reaction, graphene also shows a paper-like structure with several stacking layers of the monatomic graphene sheets (Fig. 5b). Fig. 5c and d show TEM images of G1/CIO

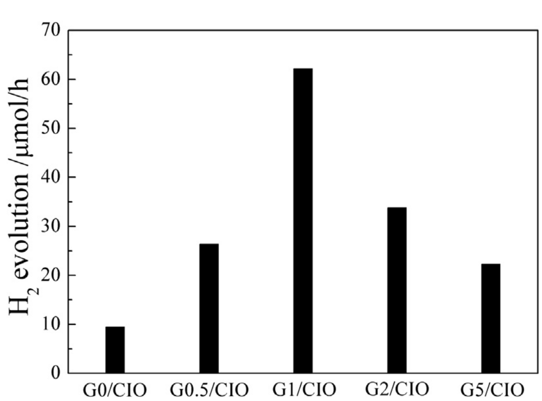

Fig. 7 – H_2 evolution of G/CIO composites with different content of graphene from CH_3OH/H_2O solution under visible light irradiation.

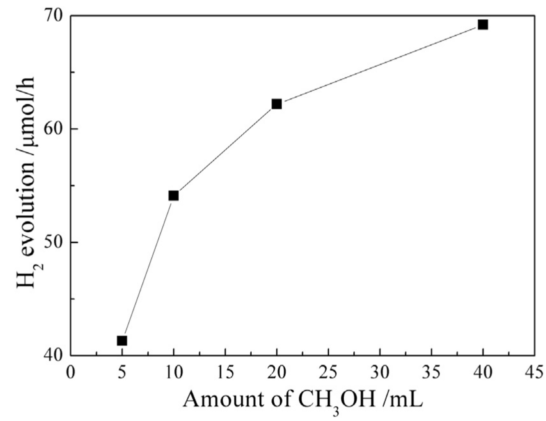

Fig. 8 – Effect of methanol concentration on the photocatalytic H_2 evolution rate over G1/CIO composite.

composite. It can be seen that a large number of rod-shaped CIO and a very small amount of spherical-shaped CIO are dispersed on the graphene sheets. CIO can interact with the graphene sheets through physisorption, electrostatic binding or through charge transfer interactions [17].

The UV–Vis absorption spectra for G/CIO composites are shown in Fig. 6a. Although visible light absorption ability of CIO is relatively weak, CIO was reported to show visible photocatalytic activity for the degradation of organic pollutants and the splitting of water. Compared with CIO, the absorption background in the visible region was enhanced for the G/CIO composites and the background became gradually stronger when the amount of graphene was increased from 0.5 to 5 wt%. This can be attributed to the presence of graphene in the G/CIO composites. A Tauc's plot [39] of the G/CIO composites is shown in Fig. 6b. The estimated band gaps from the slope are 3.42, 3.36, 3.32, 3.16 and 3.46 eV for G0.5/CIO, G1/CIO, G2/CIO, G5/CIO and pure CIO, respectively. The band gap narrowing should be attributed to the chemical bonding between CIO and graphene, which was also found in previous studies [40,41].

3.2. *Photocatalytic performance*

In this work, photocatalytic H_2 evolution activity of the prepared G/CIO composites was evaluated in CH_3OH/H_2O solution under visible-light irradiation. Control experiments showed that almost no H_2 evolution was observed in the absence of either irradiation or photocatalyst, indicating that H_2 was produced by photocatalytic reaction.

Fig. 7 shows that all the samples can produce hydrogen from CH_3OH/H_2O solution without any noble metals under visible-light irradiation. It can be seen that graphene exhibited an obvious influence on the photocatalytic activity of CIO. Even with a small content of graphene, the H_2 evolution rate was noticeably increased. For CIO alone, the amount of H_2 produced in 8 h was about 76 μmol. Along with the increase of graphene content, the photocatalytic activity of the G/CIO composites first increased and then decreased. When the graphene content in the composite increased to 1 wt%, the amount of hydrogen evolution enhanced to about 500 μmol with a rate of

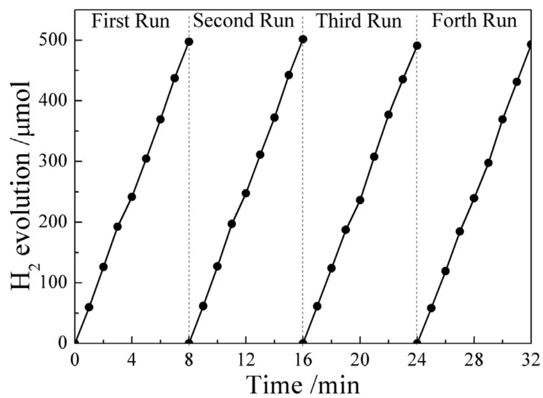

Fig. 9 – Stability of photocatalytic H_2 evolution for G1/CIO composite under visible light irradiation.

62.2 μmol h^{-1}, which is 6.6 times higher than that of pure CIO. This is attributed to two factors: (1) Graphene sheets with high surface area offer more active adsorption sites and photocatalytic reaction sites, which favor enhanced photocatalytic activity [26,28,40]. (2) In the G/CIO composites, graphene sheets serve as electron acceptor and mediator, which can reduce the probability of electron–hole recombination, improve the separation efficiency, and therefore enhance the photocatalytic activity for H_2 evolution [19,21,22,38].

However, with further increasing the amount of graphene to 2 wt%, the H_2 evolution rate was decreased to 33.8 μmol h^{-1}. A more obvious decrease in H_2 evolution rate was observed when the amount of graphene was increased to 5 wt%. The reason may be attributed to the trade-off between the excellent charge transfer capability of graphene and its detrimental effect on visible light absorption [42]. The observations are similar to the previous studies showing that a suitable loading content of graphene is crucial for optimizing the photocatalytic activity of G/CIO composites [43].

The effect of methanol concentration on the photocatalytic activity was investigated. Fig. 8 shows the H_2 evolution rate over the G1/CIO composite with different content of methanol. With the content of methanol varied from 5 to 40 mL (the volume of water was kept constant at 100 mL), the H_2 evolution rate was successively enhanced from 41.3 to 69.2 μmol h^{-1}. The observation confirms the importance of the sacrificial agent [44].

To investigate the stability of G1/CIO composite, we preformed extended reaction of 8 h in each run with the system purged between runs. No obvious deactivation of the photocatalytic activity was observed in G1/CIO composite for at least 32 h (Fig. 9), indicating the composite photocatalyst has good photocatalytic stability under visible light. The structure, morphology and composition of G1/CIO composite after 4 runs of reaction were also analyzed by XRD, TEM and XPS techniques (Fig. 10). XRD and TEM results (Fig. 10a and b) demonstrated that the crystal structure and morphology of G1/CIO composite did not change after the reaction. From Fig. 10c and d, All the Ca2p and In3d spectra show two peaks (346.5 and 350 eV with a peak splitting of 3.5 eV for the Ca2p level, 443.8 and 451.4 eV with a peak splitting of 7.6 eV for the In3d level), which indicates that the oxidation states of the element Ca and In was 2^+ and 3^+, respectively. Furthermore, there is no obvious difference in the binding energy of the C1s peaks before and after the reaction (Fig. 10e). These results

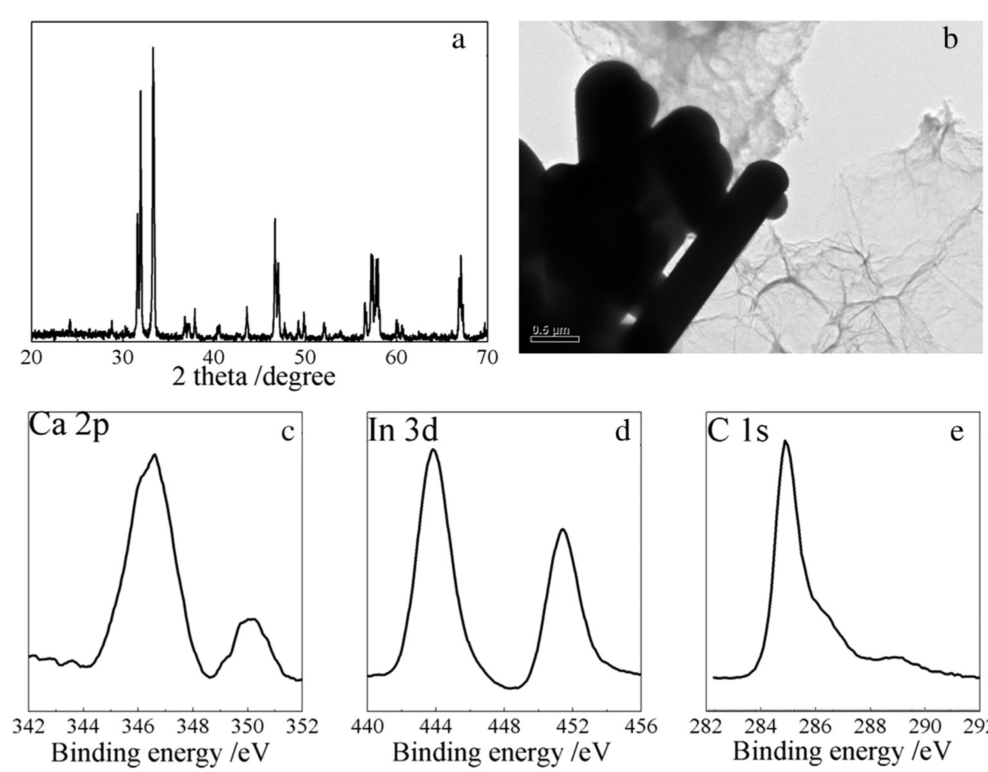

Fig. 10 – XRD patterns (a), TEM image (b) and XPS spectra (c–e) of G1/CIO composite after photocatalytic reaction for 32 h.

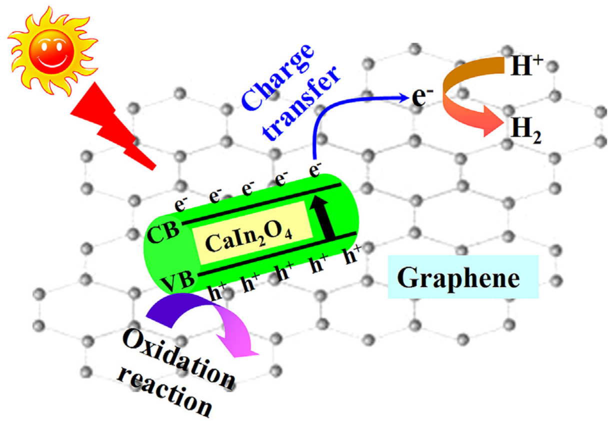

Fig. 11 – Schematic illustration of the charge separation and transportation over G/CIO composites under visible light irradiation.

indicate that the G1/CIO composite is a stable and effective photocatalyst.

It is interesting to explore the possible reasons for this considerable enhancement. A tentative mechanism for the photocatalytic H_2 evolution over G/CIO composites is proposed in Fig. 11. Under visible light irradiation, CIO absorbs visible light to generate electron–hole pairs. Then, the photogenerated electrons instantly transfer from the conduction band of CIO to the carbon atoms of graphene sheets via a percolation mechanism [45,46] and simultaneously these electrons on the surface of graphene sheets can be captured by the adsorbed H^+ to produce H_2. The holes left on the surface of CIO are scavenged by the sacrificial reagents. In this case, the introduction of graphene can effectively improve the separation efficiency of photogenerated electron–hole pairs. Meanwhile, the unique two-dimensional features of graphene sheets enable photocatalytic reactions to take place not only on the surfaces of CIO but also on the graphene sheets, thus remarkable enlarging the reaction space [21,24].

4. Conclusions

In summary, we have successfully synthesized graphene/$CaIn_2O_4$ composites as photocatalyst for water splitting under visible light irradiation. The as-prepared graphene/$CaIn_2O_4$ composites have been demonstrated to be efficient photocatalysts for H_2 evolution from CH_3OH/H_2O solution under visible light irradiation. The composite with 1 wt% graphene exhibited the highest photocatalytic activity and did not show deactivation for H_2 evolution for longer than 32 h. The results presented in this study indicated that graphene is a very promising candidate for development of visible light driven photocatalysts with efficient and stable performance.

Acknowledgments

This work was supported by National Nature Science Foundation of China (11179034, 11205159), Anhui Provincial Natural Science Foundation (1308085MB27), and National Basic Research Program of China (973 Program) (2012CB922004).

REFERENCES

[1] Fujishima A, Honda K. Electrochemical photolysis of water at a semiconductor electrode. Nature 1972;238:37–8.
[2] Linsebigler AL, Lu GQ, Yates JT. Photocatalysis on TiO_2 surface: principles, mechanisms, and selected results. Chem Rev 1995;95:735–58.
[3] Fujishima A, Zhang XT, Tryk DA. TiO_2 photocatalysis and related surface phenomena. Surf Sci Rep 2008;63:515–82.
[4] Abe R, Takami H, Murakami N, Ohtani B. Pristine simple oxides as visible light driven photocatalysts: highly efficient decomposition of organic compounds over platinum-loaded tungsten oxide. J Am Chem Soc 2008;130:7780–1.
[5] Kudo A, Omori K, Kato H. A novel aqueous process for preparation of crystal form-controlled and highly crystalline $BiVO_4$ powder from layered vanadates at room temperature and its photocatalytic and photophysical properties. J Am Chem Soc 1999;121:11459–67.
[6] Zou ZG, Ye JH, Sayama K, Arakawa H. Direct splitting of water under visible light irradiation with an oxide semiconductor photocatalyst. Nature 2001;414:625–7.
[7] Tang JW, Zou ZG, Ye JH. Efficient photocatalytic decomposition of organic contaminants over $CaBi_2O_4$ under visible-light irradiation. Angew Chem Int Ed 2004;43:4463–6.
[8] Sato J, Saito N, Nishiyama H, Inoue Y. Photocatalytic activity for water decomposition of indates with octahedrally coordinated d^{10} configuration. I. Influences of preparation conditions on activity. J Phys Chem B 2003;107:7965–9.
[9] Tang JW, Zou ZG, Yin J, Ye JH. Photocatalytic degradation of methylene blue on $CaIn_2O_4$ under visible light irradiation. Chem Phys Lett 2003;382:175–9.
[10] Tang JW, Zou ZG, Ye JH. Effects of substituting Sr^{2+} and Ba^{2+} for Ca^{2+} on the structural properties and photocatalytic behaviors of $CaIn_2O_4$. Chem Mater 2004;16:1644–9.
[11] Tang JW, Zou ZG, Katagiri M, Kako T, Ye JH. Photocatalytic degradation of MB on MIn_2O_4 (M = alkali earth metal) under visible light: effects of crystal and electronic structure on the photocatalytic activity. Catal Today 2004;93–95:885–9.
[12] Tang JW, Zou ZG, Ye JH. Kinetics of MB degradation and effect of pH on the photocatalytic activity of MIn_2O_4 (M = Ca, Sr, Ba) under visible light irradiation. Res Chem Intermed 2005;31:513–9.
[13] Chang WK, Rao KK, Kuo HC, Cai JF, Wong MS. A novel core-shell like composite In_2O_3@$CaIn_2O_4$ for efficient degradation of methylene blue by visible light. Appl Catal A 2007;321:1–6.
[14] Ge L. Preparation of novel visible-light-driven In_2O_3@$CaIn_2O_4$ composite photocatalyst by sol–gel method. J Sol-Gel Sci Technol 2007;44:263–8.
[15] Chang WK, Sun DS, Chan H, Huang PT, Wu WS, Lin CH, et al. Visible-light-responsive core-shell structured In_2O_3@$CaIn_2O_4$ photocatalyst with superior bactericidal properties and biocompatibility. Nanomed Nanotechnol 2012;8:609–17.
[16] Ding JJ, Sun S, Bao J, Luo ZL, Gao C. Synthesis of $CaIn_2O_4$ rods and its photocatalytic performance under visible-light irradiation. Catal Lett 2009;130:147–53.
[17] Williams G, Seger B, Kamat PV. TiO_2-graphene nanocomposites. UV-assisted photocatalytic reduction of graphene oxide. ACS Nano 2008;2:1487–91.
[18] Zhu MS, Chen PL, Liu MH. Graphene oxide enwrapped Ag/AgX (X = Br, Cl) nanocomposite as a highly efficient visible-light plasmonic photocatalyst. ACS Nano 2011;5:4529–36.

[19] Xiang QJ, Yu JG, Jaroniec M. Preparation and enhanced visible-light photocatalytic H_2-production activity of graphene/C_3N_4 composites. J Phys Chem C 2011;115:7355–63.
[20] Xiang QJ, Yu JG, Jaroniec M. Graphene-based semiconductor photocatalyst. Chem Soc Rev 2012;41:782–96.
[21] Zhang H, Lv XJ, Li YM, Wang Y, Li JH. P25-graphene composite as a high performance photocatalyst. ACS Nano 2010;4:380–6.
[22] Dang HF, Dong XF, Dong YC, Huang JS. Facile and green synthesis of titanate nanotube/graphene nanocomposites for photocatalytic H_2 generation from water. Int J Hydrogen Energy 2013;38:9178–85.
[23] Ng YH, Iwase A, Kudo A, Amal R. Reducing graphene oxide on a visible-light $BiVO_4$ photocatalyst for an enhanced photoelectrochemical water splitting. J Phys Chem Lett 2010;1:2607–12.
[24] Li Q, Guo BD, Yu JG, Ran JR, Zhang BH, Yan HJ, et al. Highly efficient visible-light-driven photocatalytic hydrogen production of CdS-cluster-decorated graphene nanosheets. J Am Chem Soc 2011;133:10878–84.
[25] Cheng P, Yang Z, Wang H, Cheng W, Chen MX, Shangguan WF, et al. TiO_2-graphene nanocomposites for photocatalytic hydrogen production from splitting water. Int J Hydrogen Energy 2012;37:2224–30.
[26] Tang XS, Tay QL, Chen Z, Chen Y, Goh GKL, Xue JM. CuInZnS-decorated graphene nanosheets for highly efficient visible-light-driven photocatalytic hydrogen production. J Mater Chem A 2013;1:6359–65.
[27] Xu YX, Bai H, Lu GW, Li C, Shi GQ. Flexible graphene films via the filtration of water-soluble noncovalent functionalized graphene sheets. J Am Chem Soc 2008;130:5856–7.
[28] An XQ, Yu JC, Wang Y, Hu YM, Yu XL, Zhang GJ. WO_3 nanorods/graphene nanocomposites for high-efficiency visible-light-driven photocatalysis and NO_2 gas sensing. J Mater Chem 2012;22:8525–31.
[29] Gu LA, Wang JY, Cheng H, Zhao YZ, Liu LF, Han XJ. One-step preparation of graphene-supported anatase TiO_2 with exposed {001} facets and mechanism of enhanced photocatalytic properties. ACS Appl Mater Interfaces 2013;5:3085–93.
[30] Stankovich S, Dikin DA, Piner RD, Kohlhaas KA, Kleinhammes A, Jia YY, et al. Synthesis of graphene-based nanosheets via chemical reduction of exfoliated graphite oxide. Carbon 2007;45:1558–65.
[31] Iwase A, Ng YH, Ishiguro Y, Kudo A, Amal R. Reduced graphene oxide as a solid-state electron mediator in Z-scheme photocatalytic water splitting under visible light. J Am Chem Soc 2011;133:11054–7.
[32] Zhang YH, Zhang N, Tang ZR, Xu YJ. Improving the photocatalytic performance of graphene-TiO_2 nanocomposites via a combined strategy of decreasing defects of graphene and increasing interfacial contact. Phys Chem Chem Phys 2012;14:9167–75.
[33] Liang YT, Vijayan BK, Gray KA, Hersam MC. Minimizing graphene defects enhances titania nanocomposite-based photocatalytic reduction of CO_2 for improved solar fuel production. Nano Lett 2011;11:2865–70.
[34] Gao EP, Wang WZ, Shang M, Xu JH. Synthesis and enhanced photocatalytic performance of graphene-Bi_2WO_6 composite. Phys Chem Chem Phys 2011;13:2887–93.
[35] Manna AK, Pati SK. Tuning the electronic structure of graphene by molecular charge transfer: a computational study. Chem Asian J 2009;4:855–60.
[36] Shen JF, Yan B, Shi M, Ma HW, Li N, Ye MX. One step hydrothermal synthesis of TiO_2-reduced graphene oxide sheets. J Mater Chem 2011;21:3415–21.
[37] Zhang YH, Zhang N, Tang ZR, Xu YJ. Graphene transforms wide band gap ZnS to a visible light photocatalyst. The new role of graphene as a macromolecular photosensitizer. ACS Nano 2012;6:9777–89.
[38] Wang WG, Yu JG, Xiang QJ, Cheng B. Enhanced photocatalytic activity of hierarchical macro/mesoporous TiO_2-graphene composites for photodegradation of acetone in air. Appl Catal B 2012;119–120:109–16.
[39] Kou HH, Zhang X, Jiang YM, Li JJ, Yu SJ, Zheng ZX, et al. Electrochemical atomic layer deposition of a $CuInSe_2$ thin film on flexible multi-walled carbon nanotubes/polyimide nanocomposite membrane: structure and photoelectrical characterizations. Electrochim Acta 2011;56:5575–81.
[40] Li ZX, Shen Y, Yang C, Lei YC, Guan YH, Lin YH, et al. Significant enhancement in the visible light photocatalytic properties of $BiFeO_3$-graphene nanohybrids. J Mater Chem A 2013;1:823–9.
[41] Zhang N, Yang MQ, Tang ZR, Xu YJ. CdS-graphene nanocomposites as visible light photocatalysts for redox reactions in water: a green route for selective transformation and environmental remediation. J Catal 2013;303:60–9.
[42] Mukherji A, Seger B, Lu GQ, Wang LZ. Nitrogen doped $Sr_2Ta_2O_7$ coupled with graphene sheets as photocatalysts for increased photocatalytic hydrogen production. ACS Nano 2011;5:3483–92.
[43] Zhang XY, Sun YJ, Cui XL, Jiang ZY. A green and facile synthesis of TiO_2/graphene nanocomposites and their photocatalytic activity for hydrogen evolution. Int J Hydrogen Energy 2012;37:811–5.
[44] Yi HB, Peng TY, Ke DN, Ke D, Zan L, Yan CH. Photocatalytic H_2 production from methanol aqueous solution over titania nanoparticles with mesostructures. Int J Hydrogen Energy 2008;33:672–8.
[45] Sun YF, Qu BY, Liu Q, Gao S, Yan ZX, Yan WS, et al. Highly efficient visible-light-driven photocatalytic activities in synthetic ordered monoclinic $BiVO_4$ quantum tubes-graphene nanocomposites. Nanoscale 2012;4:3761–7.
[46] Wang X, Zhi LJ, Mullen K. Transparent, conductive graphene electrodes for dye-sensitized solar cells. Nano Lett 2008;8:323–7.